EFFECTS OF THE ILLUMINATION GEOMETRY ON THE RETRIEVAL OF MIR REFLECTANCE

Renata Libonati[1,3], Carlos C. DaCamara[1], Jose Miguel C. Pereira[2], Alberto Setzer[3] and Leonardo F. Peres[3]

[1]IDL-CGUL, Faculdade de Ciências, Universidade de Lisboa, Portugal. rlsantos@fc.ul.pt, cdcamara@fc.ul.pt
[2]Department of Forestry, Instituto Superior de Agronomia, Technical University of Lisbon, Portugal. jmcpereira@isa.utl.pt [3]Instituto Nacional de Pesquisas Espaciais, Brasil. asetzer@cptec.inpe.br, lperes@cptec.inpe.br

RESUMO: Neste trabalho estudam-se as pertubaçao devidas aos efeitos da geometria de iluminação na estimativa da reflectância do infravermelho médio com ênfase na discriminação de áreas queimadas. A análise baseia-se em simulações de radiância nos canais do infravermelho-médio do sensor Moderate-resolution Imaging Spectroradiometer (MODIS) para diferentes ângulos solares e de visão. Os resultados apresentam uma forte dependência em relação ao ângulo solar zenital, sugerindo que qualquer método desenvolvido com o objetivo de separar a componente reflectiva no infravermelho médio deva considerar um limite de 45º do ângulo solar zenital.

ABSTRACT: This work focus on the perturbations induced by the effects of illumination geometry on the retrieval of middle-infrared (MIR) reflectance, with emphasis on burned area discrimination. The analysis is based on simulated radiances for different solar-viewing angles as observed by Moderate-resolution Imaging Spectroradiometer (MODIS) middle-infrared bands. The results show a strong dependence on the solar zenith angle (SZA) suggesting that any method developed with the aim of separating the reflective part of MIR signal should consider a 45° solar zenith angle cut-off.

Key-words: solar zenith angle, biomass burning, middle-infrared, burnt area, remote sensing

1. INTRODUCTION

An accurate identification of burnt areas is required for a wide range of applications from the assessment of economic losses and ecological effects up to the monitoring of land use/cover changes and the modeling of atmospheric and climatic impacts of biomass burning. Given the very broad spatial extent and the usually limited accessibility of the areas affected by fire, the use of remotely sensed data is by far the only suitable approach to collect cost-effective information at required spatial and temporal resolutions. Remote-sensing detection of burned areas requires an appropriate choice of spectral bands that are sensitive enough to changes caused by burning at the surface. These aspects also requires an appropriate knowledge of how measurements in chosen bands maybe affected by perturbing factors (Pinty and Verstraete 1992, Trigg and Flasse 2001) including changes in pre-burn surface conditions, such as the photosynthetic state and type of vegetation, as well as in atmospheric constituents above the burned surface, such as water vapor and smoke aerosols (Miura et al. 1998, Pereira 2003). Generally neglected perturbing factor, at least in burned area detection studies, is the effect due to the illumination geometry. Accordingly, this work focus on such perturbing effects of the solar zenith angle on middle-infrared (MIR) reflectance estimation with especially emphasis on burned areas. The analysis is based on simulated top of the atmosphere (TOA) radiance data as observed by Moderate-resolution Imaging Spectroradiometer (MODIS) middle-infrared band 20 for different solar-view angles and focusing on burned area studies. Data on emissivity from Johns Hopkins University (JHU) and Jet Propulsion Laboratory (JPL) spectral libraries included in the ASTER spectral library, as well as from the MODIS-UCSB spectral library, are restrict to information on spectral emissivity of different types of materials, such as vegetation, water, soil, rocks and manmade. However, to our knowledge, no assessment has been made on the measurement of emissivity from charcoal, ash or any burned material in the spectral region considered in this study. Hence, data on emissivity of charcoal in the vicinity of 3.9 μm used in the present study appears as the only available information to examine the behavior of burned materials in this spectral domain.

2. METHOD AND DATA

The radiance measured by a sensor in the middle-infrared (MIR) region of the electromagnetic spectrum contains both thermal emissive and reflective components. Thermal emission arises from atmospheric and surface thermal sources. The reflective component contains solar and thermal flux reflected by the surface and the atmosphere. The solar reflected component of MIR is of interest because of its spectral uniqueness, but it needs to be isolated from the total signal.

The general expression for satellite measured radiance at TOA level in MIR channel for a clear-sky condition may be written as a simple energy balance equation:

$$L_{\mathrm{MIR}} = t_{\mathrm{MIR}}\rho_{\mathrm{MIR}}\frac{E_{0\mathrm{MIR}}}{\pi}\mu_0 + \tau_{\mathrm{MIR}}\left[\varepsilon_{\mathrm{MIR}}B(\lambda_{\mathrm{MIR}},T_{\mathrm{S}}) + \rho_{\mathrm{MIR}}L_{\mathrm{atm,MIR}}\downarrow\right] + L_{\mathrm{atm,MIR}}\uparrow + L_{\mathrm{S}} \qquad (1)$$

where t_{MIR} is the two-way total atmospheric transmittance (sun-surface-sensor); ρ_{MIR} is the surface reflectance; $E_{0\mathrm{MIR}}$ is the exo-atmospheric irradiance; μ_0 is the cosine of the solar zenith angle; τ_{MIR} is the one-way total atmospheric transmittance (surface-sensor); $\varepsilon_{\mathrm{MIR}}$ is the surface emissivity; $B(\lambda_{\mathrm{MIR}},T_{\mathrm{S}})$ is emitted radiance given by Planck's function for the surface temperature T_{S} and central wavelength λ_{MIR}; $L_{\mathrm{atm,MIR}}\downarrow$ is the atmospheric downward thermal emission; $L_{\mathrm{atm,MIR}}\uparrow$ is the atmospheric upward thermal emission and L_{S} is the term associated with the atmospheric scattering.

The first term on the right-hand side of equation (1) represents the solar radiance that is attenuated by atmosphere in its downward path, reflected by the surface and then attenuated in its upward path to sensor. The second term represents the radiance emitted by the surface that is attenuated by the atmosphere. The third term denotes the downward atmospheric radiance that is reflected by the surface and then attenuated in its upward path to sensor. The fourth term represents the radiance emitted by the atmosphere towards the sensor. Finally, the last term is associated with atmospheric scattering.

Assuming the Earth's surface as a Lambertian emitter-reflector, we may relate the surface reflectance and emissivity as follows:

$$\rho_{\mathrm{MIR}} = 1 - \varepsilon_{\mathrm{MIR}} \qquad (2)$$

The solution of equation (1) for surface reflectance, using equation (2) and neglecting the atmospheric scattering term L_{S} is given by:

$$\rho_{\mathrm{MIR}} = \frac{L_{\mathrm{MIR}} - \tau_{\mathrm{MIR}}B(\lambda_{\mathrm{MIR}},T_{\mathrm{S}}) - L_{\mathrm{atm,MIR}}\uparrow}{t_{\mathrm{MIR}}\frac{E_{0\mathrm{MIR}}}{\pi}\mu_0 - \tau_{\mathrm{MIR}}B(\lambda_{\mathrm{MIR}},T_{\mathrm{S}}) + \tau_{\mathrm{MIR}}L_{\mathrm{atm,MIR}}\downarrow} \qquad (3)$$

It is worth noting that the accuracy of equation (3) will essentially depend on three main sources of errors, namely, the error from the atmospheric profiles, which is quantified by the error in temperature and humidity profiles, the error due to the instrument performance that is quantified by the radiometric noise and the error due to the uncertainties in the retrieval of T_{S}. In the present study, such sources of errors were not taken into account, i.e., results were generated considering that the surface temperature and the atmospheric profiles are perfectly known and do not dependent on instrument performance. Accordingly we have just examined the case when all errors are assumed to be exclusive due the inversion procedure.

We have performed radiative transfer simulations for a wide variety of atmospheric, surface and geometry conditions, including different geophysical situations observed by MODIS sensor. Simulations of observed radiances of MODIS channels 20, were obtained using MODTRAN-4 (Berk et al., 2000), a well-established radiative transfer model that allows prescribing the surface parameters as well as defining the geometrical path and sensor characteristics. The atmospheric contribution was here computed using three geographical–seasonal model atmospheres stored in MODTRAN-4, namely Mid-Latitude Summer (MLS), Mid-Latitude Winter (MLW), and Tropical (TRO), that allow covering different atmospheric conditions. The assigned land surface temperature values were based on the 2-m air temperature of each profile. The sun–viewing geometry were characterized by 3 view zenith angles (0º ,30º and 60º) and 4 solar zenith angles, namely, 0º ,30º ,45º and 60º. The charcoal spectrum was obtained at the NASA Jet Propulsion Laboratory with a Beckman UV5240 spectrophotometer, from samples of fire residues from Alta Floresta, state of Mato Grosso, Brazil. The charcoal dataset is composed by fire residues of 4 different kinds of tropical trees and in order to reduce the number of computations we have opted to use the mean of the charcoal datasets.

3. RESULTS

Performances of equation (3) are evaluated based on simulations of TOA radiances at MODIS channel 20. The retrieval errors were computed based on the differences between the values of MIR reflectance as retrieved with equation (3) and the corresponding value as prescribed in MODTRAN-4 to simulate the TOA radiances.

Figure 1 presents the obtained root mean square error (RMSE) in the retrieval of MIR reflectance for 3 different solar zenith angles as a function of the satellite viewing angle for tropical, mid-latitude summer and mid-latitude winter profile. In all cases, errors in MIR reflectance increase with solar illumination geometry. This feature reflects the fact that as the illumination angle decreases the solar contribution to MIR signal becomes less significant and therefore the radiance measured by the sensor turns out to be essentially from thermal sources. Accordingly, low sun elevations will introduce the largest errors as a consequence of the strong influence of the thermal sources when compared to the negligible contribution of solar radiation.

In the case o f the tropical profile the retrieval of MIR reflectance is more affected by the illumination geometry than for mid-latitude winter profile. For instance, for nadir, the increase in the errors from a solar zenith angle of 0º to 45º is approximately 150%, 100% and 45% for tropical, mid-latitude summer and mid-latitude winter profiles, respectively. This relatively strong dependence of the tropical and mid-latitude summer atmospheres on the illumination geometry is probably due to the presence of more water vapor in the atmosphere column.

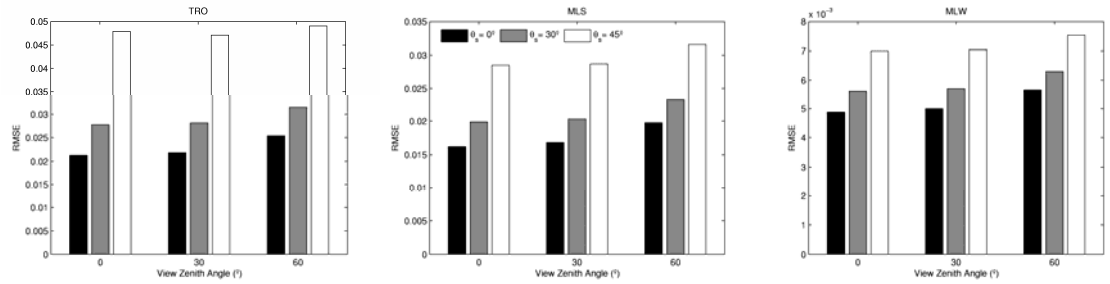

Figure 1. Dependence on satellite viewing angle of errors in the retrieval of MIR reflectance of charcoal for TRO (left panel), MLS (middle panel) and MLW (right panel) for 3 solar zenith angles (respectively, $\theta_s = 0º$ - black bar, $\theta_s = 30º$ - gray bar and $\theta_s = 45º$ - white bar).

Figure 2 illustrates the dependency on surface temperature of errors in the retrieval of MIR reflectance of charcoal for TRO (left panel), MLS (middle panel) and MLW (right panel) for 3 view angles and 4 solar zenith angles. In the case of TRO profile, a rapidly increase in the errors may be observed around 325 and 330 K for $\theta_s = 60º$. Such ill-condition behavior is due to the fact that in the denominator of the right hand site of equation 3, as temperature rises, the term $\tau_{MIR} B(\lambda_{MIR}, T_s)$ increases up to the magnitude of term $t_{MIR} \frac{E_{0MIR}}{\pi} \mu_0$ (this term decreases with the increase of θ_s). In such circumstances, the error in the retrieved reflectance due to neglecting the atmospheric scattering becomes important, because the neglected term is of the same order of magnitude as the numerator of equation (3). Accordingly in the case of low sun elevations and high temperatures, ignoring the atmospheric scattering may not have a negligible effect on the reflectance retrieval leading to a huge increase in the reflectance error.

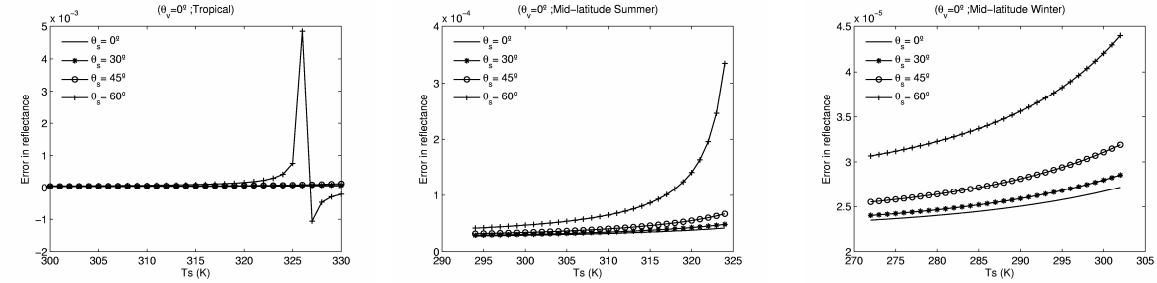

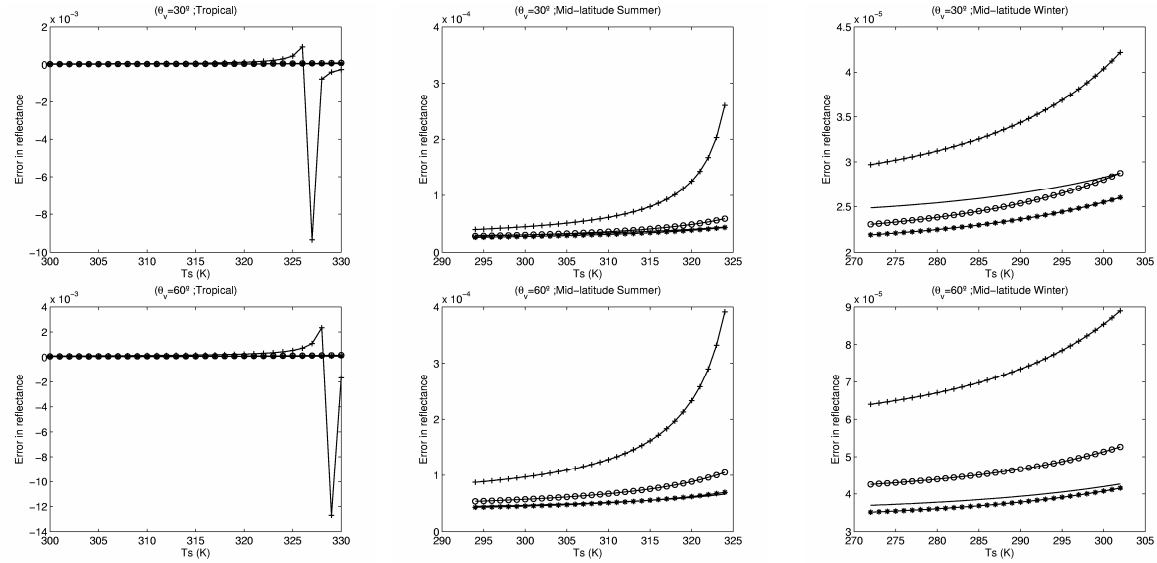

Figure 2. Dependence of land surface temperature of Errors in the retrieval of MIR reflectance of charcoal for TRO (left panel), MLS (middle panel) and MLW (right panel) for 3 view angles and 4 solar zenith angles.

4. CONCLUSIONS

Although these findings are limited to simulations with a radiative transfer model, they provide evidence on how the solar angle may perturb the retrieval of the reflectance in the middle-infrared MODIS channel 20. Ours findings demonstrate that low sun elevations of burned surfaces will introduce large errors in the retrieval of MIR reflectance, particularly in tropical environments. An important implication of these findings is that any method developed with the aim of separating the reflective part of MIR signal should consider a 45° solar zenith angle cut-off, in order to mitigate problems associated with ill-conditions at low illumination angles.

ACKNOWLEDGEMENTS: The Portuguese Foundation of Science and Technology (FCT) have supported the research performed by the first author (Grant No. SFRH/BD/21650/2005). The authors would like to thank the Faculdade de Ciências da Universidade de Lisboa and the Instituto Nacional de Pesquisas Espaciais (INPE) for providing the computing resources. The authors are indebted to Carlos Pires from University of São Paulo (USP) for providing aerosol information; to José Carlos dos Santos from the Laboratory of Combustion and Propulsion (LCP/INPE) for collecting the samples of charcoal, and Dr. Simon Hook from Jet Propulsion Laboratory (JPL/NASA) for processing the measurements of emissivity from charcoal.

5. REFERECES

BERK, A., ANDERSON, G. P., ACHARYA, P. K., CHETWYND, J. H., BERNSTEIN, L. S., SHETTLE, E. P., MATTHEW, M. W., ALDER-GOLDEN, S. M. MODTRAN4 version 2 user's manual. Air Force Research Laboratory, Space Vehicles Directorate, Air Force Material Command, Hanscom AFB, MA 01731-3010, 2000.

KIMES, D.S., 1983, Dynamics of directional reflectance factor distributions for vegetation canopies. Applied Optics, 22, pp. 1364–1372.

KLEMA, V. and LAUB, A., 1980, The singular value decomposition: its computation and some applications. IEEE Transactions on automatic control, AC-25(2), pp. 164-176.

MIURA, T., HUETE, A.R., VAN LEEUWEN, W.J.D. and DIDAN, K., 1998, Vegetation detection through smoke filled AVIRIS images: an assessment using MODIS band passes. Journal of Geophysical Research, 103, pp. 32 001–32 011.

PEREIRA, J.M.C., 2003, Remote sensing of burned areas in tropical savannas. International Journal of Wildland Fire, 12, pp. 259–270.

PERES, L. F. and DACAMARA, C. C., 2004. Inverse Problems Theory and Application: Analysis of the Two-Temperature Method for Land-Surface Temperature and Emissivity Estimation. IEEE Geoscience and Remote Sensing Letters, Vol. 1 pp. 206-210 (DOI information: 10.1109\LGRS.2004.830613).

PINTY, B. and VERSTRAETE, M., 1992, On the design and validation of bidirectional reflectance and albedo models. Remote Sensing of Environment, 41, pp. 155–167.

ROY, D. and LANDMANN, T., 2005, Characterizing the surface heterogeneity of fire effects using multi-temporal reflective wavelength data. International Journal of Remote Sensing, 26, pp. 4197–4218.

ROY, D.P., LEWIS, P.E. and JUSTICE, C.O., 2002, Burned area mapping using multi-temporal moderate spatial resolution data—a bi-directional reflectance model-based expectation approach. Remote Sensing of Environment, 83, pp. 263–286.

STROPPIANA, D., PINNOCK, S., PEREIRA, J.M.C. and GRE´GOIRE, J.M., 2002, Radiometric analysis of SPOT-VEGETATION images for burnt area detection in Northern Australia. Remote Sensing of Environment, 82, pp. 21–37.

TRIGG, S. and FLASSE, S., 2001, An evaluation of different bi-spectral spaces for detecting burned shrub-savannah. International Journal of Remote Sensing, 22, pp. 2641–2647.

TRIGG, S., ROY, D. and FLASSE, S., 2005, An in situ study of the effects of surface anisotropy on the remote sensing of burned savannah. International Journal of Remote Sensing, 26, pp. 4869–4876.